UvA-DARE (Digital Academic Repository)

The Green Bank Telescope 350 MHz Drift-scan Survey II

Data Analysis and the Timing of 10 New Pulsars, Including a Relativistic Binary

Lynch, R.S.; Boyles, J.; Ransom, S.M.; Stairs, I.H.; Lorimer, D.R.; McLaughlin, M.A.; Hessels, J.W.T.; Kaspi, V.M.; Kondratiev, V.I.; Archibald, A.M.; Berndsen, A.; Cardoso, R.F.; Cherry, A.; Epstein, C.R.; Karako-Argaman, C.; McPhee, C.A.; Pennucci, T.; Roberts, M.S.E.; Stovall, K.; van Leeuwen, J.

[Link to publication](#)

THE GREEN BANK TELESCOPE 350 MHz DRIFT-SCAN SURVEY II: DATA ANALYSIS AND THE TIMING OF 10 NEW PULSARS, INCLUDING A RELATIVISTIC BINARY

RYAN S. LYNCH[1,2], JASON BOYLES[3,4], SCOTT M. RANSOM[5], INGRID H. STAIRS[6], DUNCAN R. LORIMER[3,15],
MAURA A. MCLAUGHLIN[3], JASON W. T. HESSELS[7,8], VICTORIA M. KASPI[1], VLADISLAV I. KONDRATIEV[7,9], ANNE M. ARCHIBALD[1],
AARON BERNDSEN[6], ROGERIO F. CARDOSO[3], ANGUS CHERRY[6], COURTNEY R. EPSTEIN[10], CHEN KARAKO-ARGAMAN[1],
CHRISTIE A. MCPHEE[6], TIM PENNUCCI[2], MALLORY S. E. ROBERTS[11,12], KEVIN STOVALL[13,14], AND JOERI VAN LEEUWEN[7,8]

[1] Department of Physics, McGill University, 3600 University Street, Montreal, QC H3A 2T8, Canada; rlynch@physics.mcgill.ca
[2] Department of Astronomy, University of Virginia, P.O. Box 400325, Charlottesville, VA 22904, USA
[3] Department of Physics, West Virginia University, 111 White Hall, Morgantown, WV 26506, USA
[4] Department of Physics and Astronomy, Western Kentucky University, Bowling Green, KY 42101, USA
[5] National Radio Astronomy Observatory, 520 Edgemont Road, Charlottesville, VA 22903, USA
[6] Department of Physics and Astronomy, University of British Columbia, 6224 Agricultural Road, Vancouver, BC V6T 1Z1, Canada
[7] ASTRON, The Netherlands Institute for Radio Astronomy, Postbus 2, 7990-AA Dwingeloo, The Netherlands
[8] Astronomical Institute "Anton Pannekoek," University of Amsterdam, Science Park 904, 1098-XH Amsterdam, The Netherlands
[9] Astro Space Center of the Lebedev Physical Institute, Profsoyuznaya Street 84/32, Moscow 117997, Russia
[10] Department of Astronomy, Ohio State University, 140 West 18th Avenue, Columbus, OH 43210, USA
[11] Eureka Scientific Inc., 2452 Delmer Street, Suite 100, Oakland, CA 94602, USA
[12] Department of Physics, Ithaca College, Ithaca, NY 14850, USA
[13] Center for Advanced Radio Astronomy and Department of Physics and Astronomy, University of Texas at Brownsville, Brownsville, TX 78520, USA
[14] Department of Physics and Astronomy, University of Texas at San Antonio, San Antonio, TX 78249, USA

ABSTRACT

We have completed a 350 MHz Drift-scan Survey using the Robert C. Byrd Green Bank Telescope with the goal of finding new radio pulsars, especially millisecond pulsars that can be timed to high precision. This survey covered ∼10,300 deg^2 and all of the data have now been fully processed. We have discovered a total of 31 new pulsars, 7 of which are recycled pulsars. A companion paper by Boyles et al. describes the survey strategy, sky coverage, and instrumental setup, and presents timing solutions for the first 13 pulsars. Here we describe the data analysis pipeline, survey sensitivity, and follow-up observations of new pulsars, and present timing solutions for 10 other pulsars. We highlight several sources—two interesting nulling pulsars, an isolated millisecond pulsar with a measurement of proper motion, and a partially recycled pulsar, PSR J0348+0432, which has a white dwarf companion in a relativistic orbit. PSR J0348+0432 will enable unprecedented tests of theories of gravity.

Key words: pulsars: individual (J0348+0432, J0458−0505, J1501−0046, J1518−0627, J1547−0944,
J1853−0649, J1918−1052, J1923+2515, J2013−0649, J2033+0042) – surveys

1. INTRODUCTION

The vast majority of observed neutron stars in the Galaxy manifest themselves as radio pulsars. The extremely high rotational stability of pulsars, and especially millisecond pulsars (MSPs), make them unrivaled laboratories for studying a wide range of astrophysical phenomena. Most pulsars have been discovered in large-area surveys, but most of these have focused on southern declinations or narrow regions around the Galactic plane. There is a need to find more pulsars in the northern sky, particularly high-precision MSPs that can be included in a pulsar timing array to detect gravitational waves (e.g., Jenet et al. 2009). The 100 m Robert C. Byrd Green Bank Telescope (GBT) is one of the best telescopes in the world for finding and studying pulsars and a visible-sky pulsar survey using the GBT is underway (the Green Bank North Celestial Cap survey).

During the northern summer of 2007 the azimuth track of the GBT underwent repair, making normal operations impossible.[16] Our team took advantage of the situation by completing the GBT 350 MHz Drift-scan Survey between May and August. Because the GBT was unable to move in azimuth, we observed

at a number of fixed elevations and allowed the sky to drift through the telescope beam at the sidereal rate. This survey was one of several low-frequency GBT surveys that are optimized for finding bright, nearby pulsars, with an emphasis on MSPs. These surveys have either been completed (Hessels et al. 2008), are ongoing, or are planned for the future. We collected over 1491 hr of data totaling 134 TB. Approximately 30 TB of these data are being analyzed by the Pulsar Search Collaboration,[17] an educational initiative that actively involves high school students and teachers in research under the guidance of a team of astronomers (Rosen et al. 2010). For the remainder of this paper we discuss only the ∼100 TB of the data that we have analyzed ourselves. All of these data have been fully processed and we have discovered 31 new pulsars, including 10 recycled pulsars (7 of which are MSPs with $P < 10$ ms). We have derived full timing solutions for 25 of these new pulsars. The first 13 pulsars are being presented in a companion paper (Boyles et al. 2013, hereafter Paper I), along with a detailed description of the survey strategy, sky coverage, and instrumental setup. We present timing solutions for an additional 10 pulsars here and describe the survey pipeline and data analysis in detail. An earlier-discovered Drift-scan pulsar, PSR J1023 + 0038, has been discussed elsewhere (see Archibald et al. 2009, 2010), while another MSP, PSR J2256−1024, will be

---

[15] Also adjunct at the National Radio Astronomy Observatory, Green Bank, WV 24944, USA.
[16] A history of the track repair can be found at http://www.gb.nrao.edu/gbt/track.shtml.

[17] http://www.pulsarsearchcollaboration.com/

presented in a future paper (I. H. Stairs et al., in preparation). In Section 2 we explain how the data were divided into regions on the sky, interference removal, our de-dispersion scheme, and search strategies. In Section 3 we describe our approximate survey sensitivity and the effects of scattering. In Section 4 we describe how we confirmed candidate pulsars and our follow-up observations. In Section 5 we present timing solutions and discuss some interesting individual systems. A summary can be found in Section 6.

2. DATA ANALYSIS

The Drift-scan Survey covered $\sim$10,300 deg^2. A detailed description of the survey strategy, sky coverage, and instrumental setup can be found in Paper I. Here we focus on the data reduction and search techniques. All data were processed using the PRESTO[18] software suite (Ransom 2001).

2.1. Pseudo-pointings and Interference Excision

Data were collected while the azimuth track of the GBT was being repaired, so the telescope was locked at constant azimuth. Different regions of the sky were observed by changing the elevation of the telescope and allowing the sky to drift through the telescope beam at the sidereal rate. The time for a given point on the sky to pass through the beam is

$$t \simeq \frac{b}{\mathcal{R}_{\mathrm{sid}} \cos \delta}, \quad (1)$$

where $b = 36'$ is the FWHM of the GBT beam at 350 MHz, $\mathcal{R}_{\mathrm{sid}} = 15'$ minute^{-1} is the sidereal rate, and δ is the declination. The survey covered $-8° \lesssim \delta \lesssim +38°$ and $-21° \lesssim \delta \lesssim +38°$, depending on the azimuth of the telescope (see Paper I for details). Although the telescope was not actually tracking the sky, we defined an individual *pseudo-pointing* to be a continuous block of data $\sim$140 s in duration. Each pseudo-pointing overlapped with the preceding one by 70 s, so that all of our data were processed as part of two different pseudo-pointings.

The raw data were collected using the GBT Pulsar Spigot back end (Kaplan et al. 2005). The Spigot uses autocorrelation chips that each work on three-level raw samples and create an adjustable number of lags. These are then integrated into either 8 or 16 bit values, depending on the mode. The center frequency of the observations was 350 MHz and the bandwidth was 50 MHz. Most of our observations were made using the 8 bit mode that split the band into 2048 lags which were fast Fourier transformed to synthesize 2048 frequency channels, each with a width of 24.4 kHz, and recorded every 81.92 μs. A relatively small amount of data was taken early in the survey using the 16 bit, 1024 channel mode with the same sampling time. Hence, each 140 s block of data consisted of roughly 1.7 million spectra.

Each pseudo-pointing was independently analyzed for radio frequency interference (RFI) using the rfifind tool from PRESTO. Data were broken into blocks roughly 2 s long while maintaining the full frequency resolution. The total power, mean, and variance in both the time and frequency domain were calculated for each data block and compared to the median quantity for the entire pseudo-pointing. A time/frequency block was flagged as RFI and masked out (i.e., set to zero) in future analysis if the value of total power, mean power, or variance was

greater than ten/four standard deviations from the median values for the entire pseudo-pointing. If more than 30%/70% of time intervals/channels were flagged, then all remaining intervals/channels were masked out as well, under the assumption that they probably contained RFI just below our cutoff threshold. In addition to blindly searching for RFI, the Fourier spectra were de-reddened and persistent, well-known sources of interference (e.g., the 60 Hz signal from AC power sources) were explicitly removed from the power spectra of each pseudo-pointing. Despite the fact that there was significant construction on site due to the track repair, our data were remarkably free of RFI. For example, the median masking fraction was 0.56% and only 0.2% of the data had a masking fraction greater than 30%. We are confident that we reached the noise limit for the vast majority of our survey (see Section 3).

2.2. De-dispersion

Free electrons in the interstellar medium give rise to a frequency-dependent dispersive time delay which, if left uncorrected, will make it virtually impossible to find new pulsars. The magnitude of the delay between two frequencies, ν_1 and ν_2, is

$$t_{\mathrm{DM}} \simeq 4.15 \times 10^3 \text{ s} \times \mathrm{DM} \times \left[\left(\frac{\nu_1}{\mathrm{MHz}} \right)^{-2} - \left(\frac{\nu_2}{\mathrm{MHz}} \right)^{-2} \right], \quad (2)$$

where DM is the dispersion measure in units of pc cm^{-3}. After applying appropriate shifts to each frequency channel, we summed over frequency to create de-dispersed time series. Each time series was transformed to the solar system barycenter using the DE200 ephemeris (the default used by PRESTO) and the dispersion delay was removed (i.e., as if the signal had infinite frequency). We note that we used the DE405 ephemeris for barycentering when deriving pulse times of arrival (TOAs, see Section 4.1).

The finite size of a frequency channel will still induce a smearing given by

$$t_{\mathrm{chan}} \simeq 8.3 \times 10^3 \text{ s} \left(\frac{\mathrm{DM}\Delta\nu_{\mathrm{chan}}}{\nu^3} \right), \quad (3)$$

where $\Delta\nu_{\mathrm{chan}}$ is the channel width and ν is the channel center frequency (both in megahertz). For our primary observing mode with 24.4 kHz channels centered between 325 and 350 MHz, $t_{\mathrm{chan}} \approx (3.8 \text{ to } 5.9) \mu\text{s} \times \mathrm{DM}$.

Since the DM of a pulsar is not known a priori, we created de-dispersed time series for each pseudo-pointing over a range of DMs, from 0 to $\sim$1000 pc cm^{-3}, which is a factor of three to four larger than the maximum DMs predicted by the NE2001 model (Cordes & Lazio 2002) in the low Galactic latitude regions of the survey. The step size between subsequent trial DMs (ΔDM) was chosen such that over the entire band $t_{\Delta\mathrm{DM}} \simeq t_{\mathrm{chan}}$. This ensures that the maximum extra smearing caused by any trial DM deviating from the source DM by ΔDM is less than the intra-channel smearing.[19] To increase computational efficiency, the data were down-sampled in time by adding 2^n samples together (where n is an integer) when $t_{\mathrm{chan}} \geqslant 2^n \times 81.92 \mu\text{s}$.

2.3. Search Algorithms

2.3.1. Periodic Sources

Each RFI-cleaned, de-dispersed time series was Fourier transformed and searched for periodic signals. As mentioned in

---

[18] http://www.cv.nrao.edu/~sransom/presto/

[19] De-dispersion plans were generated using the DDplan.py tool in PRESTO.

Section 2.1, known sources of RFI were explicitly removed from the Fourier spectrum, so there is a very small chance ($\sim$0.006%) that a pulsar with a spin frequency very close to known RFI could have also been removed. Acceleration searches for isolated and binary pulsars were carried out in the Fourier domain (Ransom et al. 2002) for signals with a maximum drift of $z_{\max} = \pm 50/n_{\rm harm}$ Fourier bins, where $n_{\rm harm}$ is the highest harmonic where the pulsar is detected. This corresponds to a physical acceleration of

$$A_{\max} = \frac{z_{\max} c P}{n_{\rm harm} t_{\rm int}^2}, \tag{4}$$

where c is the speed of light, P is the spin period of the pulsar, and $t_{\rm int} = 140$ s is the effective integration time (Ransom et al. 2002). For a $P = 2$ ms pulsar detected with up to eight harmonics, $A_{\max} \approx 24$ m s^{-2}. Acceleration searches used up to eight summed harmonics, but we also carried out searches for unaccelerated pulsars ($z = 0$) using up to 16 summed harmonics. Only powers-of-two numbers of harmonics were summed.

To filter out spurious and low-significance signals, only candidates that appeared in at least two time series of different DMs passed to the next stage of consideration. We also filtered duplicate signals (keeping only those with the highest signal-to-noise ratio (S/N)) that were within ± 1.1 Fourier bins of each other in different DM time series, as well as those that were harmonically related to each other. We folded up to 20 of the remaining candidates from the zero-acceleration searches and up to 10 from the high-acceleration searches if their Fourier power was at least 6σ above the Gaussian-equivalent noise level. We used the `prepfold` routine in `PRESTO` to fold the full resolution data at the nominal P, period derivative ($\dot{P}$), and DM as determined by our searches. Our folding code refined these values and created diagnostic plots that were then saved for human inspection.

2.3.2. Single-pulse Sources

We searched for bright single pulses using `single_pulse_search.py` in `PRESTO`. Each time series was smoothed using a piecewise linear fit to the data, where each piece was 2000 points long. The smoothed data were then correlated with boxcar functions of varying widths,[20] which acted as matched filters to individual pulses. We recorded all single pulses with a signal-to-noise ratio, S/N $\geqslant 5$ and created diagnostic plots for all pulses with S/N $\geqslant 5.5$. These plots were then saved for human inspection. In addition, an automated algorithm was used to flag pseudo-pointings with promising candidates, which were then inspected in greater detail. Five rotating radio transients (RRATs) have been discovered in this survey and a further 26 candidates have been identified and await confirmation. These discoveries and the automated algorithm used to help identify them will be presented in a forthcoming paper (C. Karako-Argaman et al., in preparation).

3. SURVEY SENSITIVITY

Following Dewey et al. (1985) and Lorimer & Kramer (2005), the sensitivity of a pulsar survey may be written in terms of the phase-averaged limiting flux density

$$S_{\nu,\min} = \frac{\beta}{\epsilon} \frac{({\rm S/N_{min}}) T_{\rm sys}}{G \sqrt{n_p t_{\rm int} \Delta \nu}} \sqrt{\frac{W}{P - W}}, \tag{5}$$

Table 1
Parameters of the GBT 350 MHz Drift-scan Survey

Parameter	Value
ADC conversion factor, β	1.16
Signal-to-noise threshold, S/N$_{\min}$	6.0
Receiver temperature, $T_{\rm rec}$ (K)	46
Telescope gain, G (K Jy^{-1})	2.0
Number of summed polarizations, n_p	2
Length of pseudo-pointing, $t_{\rm int}$ (s)	140
Bandwidth, Δf (MHz)	50
Number of frequency channels, $n_{\rm chan}$	2048[a]
Sampling time, $t_{\rm samp}$ (μs)	81.92

Note. [a] A small amount of data was recorded with 1024 frequency channels early in the survey.

where ϵ is a degradation factor (discussed below), $\beta = 1.16$ is a correction factor that accounts for digitization losses, S/N$_{\min}$ is the S/N threshold, $T_{\rm sys}$ is the total system temperature, G is the telescope gain, n_p is the number of summed polarizations, $t_{\rm int}$ is the integration time, $\Delta \nu$ is the bandwidth, and W is the total pulse width (see Table 1 for relevant values). The degradation factor ϵ accounts for drift of the pulsar through the telescope beam, which is not uniform in sensitivity. For a Gaussian primary beam

$$\epsilon \propto \int_0^{t_{\rm int}} e^{-r^2(t)/f^2} \, dt, \tag{6}$$

where $r(t)$ is the distance from the beam center and $f = b/(2\sqrt{\ln 2})$. From simple geometry, $r^2(t) = y^2 + (b/2 - \dot{x}t)^2$, where y and x are the distances from the beam center in right ascension and declination, respectively, and $\dot{x}$ is the drift rate. We normalize ϵ such that a pulsar at the center of the beam *for an entire integration* has $\epsilon = 1$. For reference, a pulsar that crosses the beam center will have $\epsilon = 0.81$.

The system temperature is a sum of several factors, including the receiver temperature ($T_{\rm rec}$) and the sky temperature ($T_{\rm sky}$). The 350 MHz receiver[21] of the GBT has a nominal $T_{\rm rec} = 23$ K. The Galactic synchrotron emission contributes heavily to $T_{\rm sky}$, but this depends on sky position. Most of our survey was at high Galactic latitudes, where the synchrotron emission adds $\sim$30–50 K at 350 MHz (Haslam et al. 1982). Our line of sight through the Galaxy also affects our sensitivity by increasing scattering and dispersion, both of which contribute to the observed pulse width. The typical maximum predicted DM at the high Galactic latitudes we cover is $\sim$60 pc cm^{-3}. According to the NE2001 model, this corresponds to a scattering time $\sim$0.08 ms at 350 MHz, though observed scattering times may differ from predictions by an order of magnitude or more. Obviously, DM effects become much worse at low Galactic latitudes. Figure 1 shows approximate sensitivity curves for various combinations of y (the minimum offset from the beam center), $T_{\rm sys}$, and DM. These calculations do not take the effects of RFI into account, but as we describe in Section 2.1, the survey did not suffer greatly from RFI contamination.

4. CANDIDATE CONFIRMATION AND FOLLOW-UP

Periodic and single-pulse candidates from each pseudo-pointing were judged by eye. Folded candidates were usually

---

[20] The boxcar functions had a maximum width of either $150 \times n \times dt$ or 0.1 s, whichever was greater, where n is the down-sampling factor.

[21] We have folded the receiver spillover and cosmic microwave background into this number. Characteristics of the GBT receivers are available on the NRAO Web site (http://www.gb.nrao.edu/astronomers.shtml).
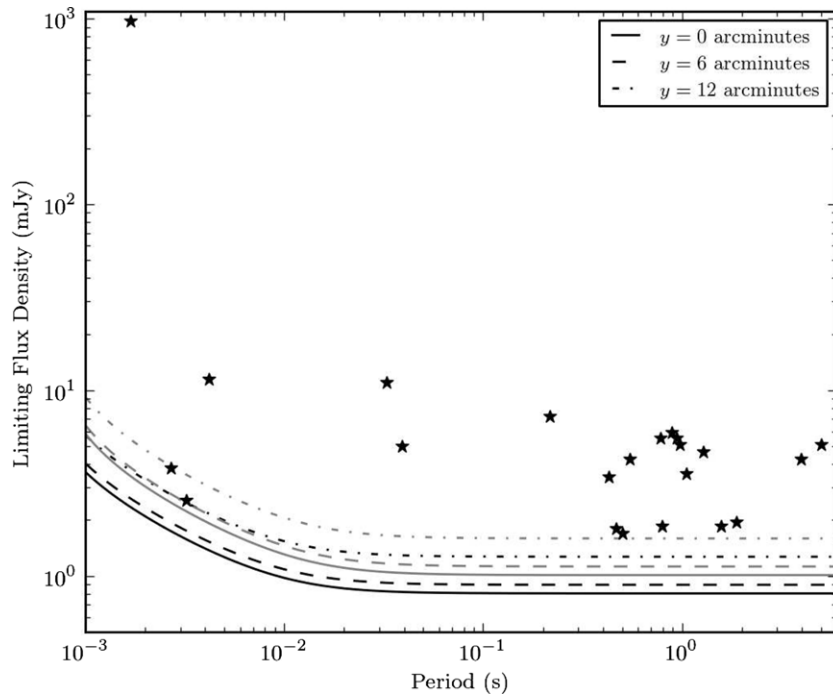
Figure 1. Approximate phase-averaged limiting flux density of our survey. Black curves are for $T_{sys} = 75$ K and DM $= 30$ pc cm^{-3}, while gray curves are for $T_{sys} = 100$ K and DM $= 75$ pc cm^{-3}. The smallest offset from the center of the telescope beam is y.

judged on three main criteria: (1) distinct peaking of the signal's significance at DMs greater than 0 pc cm^{-3}, (2) broadband emission (allowing for the possibility of regions of enhanced/diminished flux due to interstellar scintillation), and (3) fairly persistent emission in time (allowing for eclipses and nulls and accounting for the roll-off in sensitivity near the edges of the telescope beam). In the case of single-pulse candidates, we looked for pulses that peaked at a non-zero DM and that decreased in significance away from this peak. Multiple single pulses at the same DM were also an obvious indicator of a good candidate.

Promising candidates were confirmed in follow-up observations with the GBT, after which we began regular timing observations. To improve the quality of initial timing solutions, new pulsars had their sky positions refined by observing at a grid of locations with smaller GBT beams at successively higher frequencies (Morris et al. 2002). We used a number of dense observations early in the campaigns to characterize the orbits of binary pulsars. The majority of timing observations were carried out at 820 MHz, but most pulsars were also observed at other frequencies, allowing us to explore their spectral properties. We also started using the new Green Bank Ultimate Pulsar Processing Instrument[22] (GUPPI; DuPlain et al. 2008) in 2008 October. Compared to the Spigot back end, GUPPI offers larger bandwidth, better frequency and time resolution, higher dynamic range, and greater resilience to strong RFI.

4.1. Pulsar Timing Analysis

All of the new pulsars were observed regularly with the GBT as part of our timing campaign. Long-period pulsars (with $P > 0.1$ s) were observed for a minimum of about 11 months, while MSPs and recycled pulsars were observed for a minimum of 20. Each pulsar was typically observed for 10–15 minute

per observing session. High-S/N average pulse profiles were created for each observing frequency by summing data from multiple observations. We created standard pulse profiles by fitting one or more Gaussians to these average pulse profiles using a least-squares minimization routine.[23] These standard profiles were used to compute pulse TOAs using either PRESTO or PSRCHIVE[24] (Hotan et al. 2004; depending on data format) by cross-correlation in the Fourier domain. We typically obtained two TOAs per observation for isolated pulsars and four to six TOAs per observation for binary pulsars, ensuring good sampling of the orbit. Phase connected timing solutions were created using the TEMPO[25] software package and the DE405 solar system ephemeris. All of our timing solutions are referenced to UTC(NIST). All the pulsars timed here have timing solutions with reduced $\chi^2 > 1$. Since we observe no unmodeled trends in our timing residuals, this is probably due to an underestimate of individual TOA uncertainties. As is standard practice, we multiplied all TOA uncertainties by an "error factor," such that the reduced $\chi^2 = 1$.

4.2. Flux Measurements

Mean flux densities were estimated by assuming that the off-pulse root mean square (rms) noise level was described by the radiometer equation,

$$\sigma = \frac{\beta T_{sys}}{G \sqrt{n_p \Delta \nu \, t_{int}}}, \qquad (7)$$

where T_{sys} is the total system temperature. To ensure a proper estimate of the rms noise level, we fit a third-order polynomial to the off-pulse region and then subtracted this to create a flat off-pulse baseline. It is important to keep in mind, however,
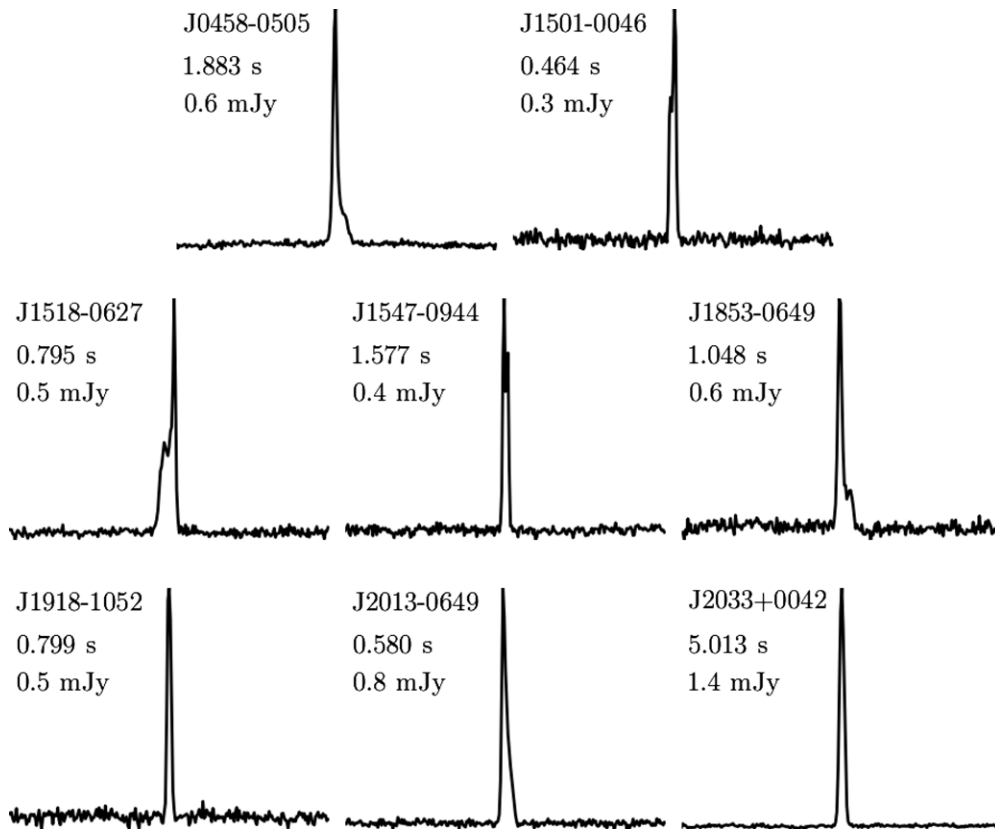

Figure 2. Integrated 820 MHz pulse profiles for the newly discovered long-period pulsars presented here. All profiles show one full rotation of the pulsar (i.e., from phase 0–1) with 256 phase bins. The profiles were made by adding all the RFI-free observations for each pulsar and were used to create standard pulse profiles at 820 MHz. Pulse periods and mean flux densities are also given.

that observed pulsar fluxes are variable due to interstellar scintillation. The values that we report here are determined by averaging several observations but should be treated only as representative. We also calculated the spectral index when flux density estimates were available for multiple frequencies. We did this by fitting a standard power law to the flux density estimates, typically at 350 MHz and 820 MHz, assuming $S_\nu \propto \nu^\alpha$. The average for the pulsars presented here is $\langle \alpha \rangle = -1.7$, which is very similar to the average value presented in Lorimer et al. (1995).

We also attempted to measure the rotation measure (RM) whenever fully calibrated polarization data were available (which was at least once for each pulsar). We searched over a wide range of RMs, from ± 1000 rad m^{-2}. We could only detect a significant RM for a subset of pulsars. Those pulsars without reported RMs are probably weakly polarized sources.

5. RESULTS

A total of 31 new pulsars have been discovered thus far in the Drift-scan Survey. The first 13 are presented in Paper I and 10 are discussed here. As mentioned in Section 1, PSR J1023+0038 has been discussed elsewhere by Archibald et al. (2009, 2010), while another MSP, PSR J2256−1024, will be presented in a future paper (I. H. Stairs et al., in preparation). Full timing solutions have not been obtained for the six most recently discovered pulsars and these will be presented in future work. The 10 pulsars presented here include eight long-period, isolated pulsars, one mildly recycled binary pulsar, and one isolated MSP. Of these 10 pulsars, 7 were detected independently in our searches for single pulses. Full timing solutions and other

properties for the long-period pulsars are presented in Table 2 and for the recycled pulsars in Table 3. Integrated pulse profiles can be seen in Figures 2 and 3 and post-fit timing residuals are shown in Figure 4. We discuss some individual systems in greater detail below.

5.1. PSR J0348 + 0432: A Relativistic Binary with a Low-mass Companion

PSR J0348 + 0432 (hereafter J0348) is a mildly recycled binary pulsar with $P = 39.1$ ms. The low magnetic field of J0348 ($B_{\rm surf} = 3.1 \times 10^9$ G) indicates that it is indeed partially recycled and not a young pulsar.[26] The DM of J0348 is 40.5 pc cm^{-3} and the DM-derived distance is 2.1 kpc. The orbital period of this system is 2.4 hr, and only three pulsars with $P < 40$ ms outside of globular clusters have shorter periods. If we assume a mass of 1.4 $M_\odot$ for J0348 then the observed mass function, $f(M) = 2.9 \times 10^{-4}$, implies a minimum companion mass of 0.086 $M_\odot$. We searched for and identified an optical counterpart to J0348 in the Sloan Digital Sky Survey with corrected SDSS magnitudes $u' = 21.84 \pm 0.19$, $g' = 20.71 \pm 0.03$, $r' = 20.60 \pm 0.03$, $i' = 20.69 \pm 0.05$, and $z' = 20.40 \pm 0.15$. More detailed spectroscopic follow-up with the Apache Point 3.5 m telescope and the Very Large Telescope have shown that the companion to J0348 is a low-mass white dwarf. The combination of a neutron star and low-mass white dwarf in a tight, relativistic orbit is unique among pulsars and makes J0348 an excellent laboratory for testing general

---

[26] Although we have not measured proper motion and cannot calculate its contribution to $\dot{P}_{\rm obs}$, it is certainly not sufficient to increase the $B_{\rm surf}$ by several orders of magnitude.

Table 2
Parameters of Newly Discovered Long-period Pulsars

Parameter	PSR J0458−0505	PSR J1501−0046	PSR J1518−0627
Timing parameters			
Right ascension (J2000)	04:58:37.121(26)	15:01:44.9558(94)	15:18:59.1104(80)
Declination (J2000)	−05:05:05.1(4.0)	−00:46:23.52(88)	−06:27:07.70(66)
Pulsar period (s)	1.88347965849(18)	0.4640368139284(82)	0.7949966745699(78)
Period derivative (s s^{-1})	5.3(1.5)×10^{-16}	2.391(60)×10^{-16}	4.179(56)×10^{-16}
Dispersion measure (pc cm^{-3})	47.806(32)	22.2584(90)	27.9631(98)
Reference epoch (MJD)	55178.0	55170.0	55170.0
Span of timing data (MJD)	55006–55349	55006–55335	55006–55335
Number of TOAs	22	39	43
rms residual (μs)	716	172	175
Error factor	2.967	1.095	1.050
Derived parameters			
Galactic longitude (deg)	204.14	356.58	355.15
Galactic latitude (deg)	−27.35	48.05	41.0
DM-derived distance (kpc)	2.6	1.4	1.6
Surface magnetic field (10^{12} G)	1.0	0.33	0.58
Spin-down luminosity (10^{32} erg s^{-1})	0.032	0.95	0.33
Characteristic age (Myr)	56	31	30
820 MHz FWHM	0.014	0.022	0.012
820 MHz flux density (mJy)	0.5	0.3	0.4
Spectral index	−1.6	−2.1	−1.8

Parameter	PSR J1547−0944	PSR J1853−0649	PSR J1918−1052
Timing parameters			
Right ascension (J2000)	15:47:46.058(36)	18:53:25.422(36)	19:18:48.247(13)
Declination (J2000)	−09:44:7.8(3.2)	−06:49:25.9(2.6)	−10:52:46.38(66)
Pulsar period (s)	1.576924632943(44)	1.048132105087(54)	0.798692542358(15)
Period derivative (s s^{-1})	2.938(36)×10^{-15}	1.548(44)×10^{-15}	8.653(15)×10^{-16}
Dispersion measure (pc cm^{-3})	37.416(22)	44.541(36)	62.73(80)
Reference epoch (MJD)	55170.0	55170.0	55026.0
Span of timing data (MJD)	55006–55335	54976–55335	54712–55339
Number of TOAs	22	24	26
rms residual (μs)	338	588	394
Error factor	1.630	2.150	2.480
Derived parameters			
Galactic longitude (deg)	358.31	27.08	26.23
Galactic latitude (deg)	33.57	−3.55	−10.96
DM-derived distance (kpc)	1.9	1.5	2.1
Surface magnetic field (10^{12} G)	2.2	1.3	0.84
Spin-down luminosity (10^{32} erg s^{-1})	0.30	0.53	0.67
Characteristic age (Myr)	8.5	11	15
820 MHz FWHM	0.019	0.015	0.015
820 MHz flux density (mJy)	0.4	0.5	0.4
Spectral index	−1.8	−2.3	· · ·
Rotation measure (rad m^{-2})	· · ·	34.7(3.2)	−47.6(6.0)

Parameter	PSR J2013−0649	PSR J2033+0042
Timing parameters		
Right ascension (J2000)	20:13:17.7507(38)	20:33:31.11(12)
Declination (J2000)	−06:49:05.39(32)	00:42:22.0(8.0)
Pulsar period (s)	0.5801872690010(34)	5.01339800063(90)
Period derivative (s s^{-1})	6.007(24)×10^{-16}	1.013(78)×10^{-14}
Dispersion measure (pc cm^{-3})	63.36(10)	37.84(13)
Reference epoch (MJD)	55172.0	55172.0
Span of timing data (MJD)	55005–55339	55005–55339
Number of TOAs	45	22
rms residual (μs)	150	2195
Error factor	1.370	4.680
Derived parameters		
Galactic longitude (deg)	36.17	45.88
Galactic latitude (deg)	−21.29	−22.2
DM-derived distance (kpc)	3.0	1.9
Surface magnetic field (10^{12} G)	0.60	7.2

6

Table 2
(Continued)

Parameter	PSR J2013−0649	PSR J2033+0042
Spin-down luminosity (10^{32} erg s^{-1})	1.2	0.032
Characteristic age (Myr)	15	7.8
820 MHz FWHM	0.017	0.018
820 MHz flux density (mJy)	0.6	1.2
Spectral index	. . .	−1.7
Rotation measure (rad m^{-2})	. . .	−71.2(2.2)

Notes. Numbers in parentheses are 1σ uncertainties as determined by TEMPO; although we have scaled the TOA uncertainties by the error factors reported, we have not doubled the nominal TEMPO uncertainties as is sometimes done in these cases. Flux density estimates typically have a 20%–30% relative uncertainty due to scintillation. All timing solutions use the DE405 solar system ephemeris and the UTC(NIST) time system. Derived quantities assume an $R = 10$ km neutron star with $I = 10^{45}$ gm cm^2 (see Lorimer & Kramer 2005). The DM-derived distances were calculated using the NE2001 model of Galactic free electron density, and have typical errors of ∼20% (Cordes & Lazio 2002).

Table 3
Parameters of Newly Discovered Short-period Pulsars

Parameter	PSR J0348+0432	PSR J1923+2515
	Timing parameters	
Right ascension (R.A.; J2000)	03:48:43.63817(33)	19:23:22.494560(76)
Declination (decl.; J2000)	04:32:11.449(10)	25:15:40.6436(14)
R.A. proper motion (mas yr^{-1})	. . .	−6.2(2.4)
Decl. proper motion (mas yr^{-1})	. . .	−23.5(7.0)
Pulsar period (s)	0.039122656280156(10)	0.00378815551961303(52)
Period derivative (s s^{-1})	2.417(16)×10^{-19}	9.42(14)×10^{-21}
Dispersion measure (pc cm^{-3})	40.56(11)	18.85766(19)
Reference epoch (MJD)	55278.0	55322.0
Span of timing data (MJD)	54873–55682	55005–55639
Number of TOAs	183	153
Error factor	1.657	1.245
rms residual (μs)	10.33	5.0
	Binary parameters	
Binary model	ELL1	. . .
Orbital period (days)	0.10242406134(30)	. . .
Projected semi-major axis (lt-s)	0.1409842(34)	. . .
Epoch of ascending node (MJD)	54889.70532337(65)	. . .
First Laplace parameter	$<5.0 \times 10^{-5}$	. . .
Second Laplace parameter	$<6.3 \times 10^{-5}$	. . .
	Derived parameters	
Orbital eccentricity	$<8.1 \times 10^{-5}$	. . .
Mass function ($M_\odot$)	0.000286807(20)	. . .
Minimum companion mass ($M_\odot$)	0.086	. . .
Galactic longitude (deg)	183.34	58.95
Galactic latitude (deg)	−36.77	4.75
DM-derived distance (kpc)	2.1	1.6
Transverse velocity (km s^{-1})	. . .	188(46)
Shklovskii effect (s s^{-1})	. . .	8.9(4.7)×10^{-21}
Intrinsic spin-down (s s^{-1})	. . .	$<5.3 \times 10^{-21}$[a]
Surface magnetic field (10^9 G)	3.1	<1.4[a]
Spin-down luminosity (10^{32} erg s^{-1})	1.6	<38[a]
Characteristic age (Gyr)	2.6	>11[a]
820 MHz FWHM	0.016	0.142
820 MHz flux density (mJy)	1.8	0.6
Spectral index	−1.2	−1.7
Rotation measure (rad m^{-2})	49.5(13)	10.8(3.8)

Notes. Numbers in parentheses are 1σ uncertainties as determined by TEMPO; although we have scaled the TOA uncertainties by the error factors reported, we have not doubled the nominal TEMPO uncertainties as is sometimes done in these cases. Flux density estimates typically have a 20%–30% relative uncertainty due to scintillation. All timing solutions use the DE405 solar system ephemeris and the UTC(NIST) time system. Derived quantities assume an $R = 10$ km neutron star with $I = 10^{45}$ gm cm^2 (see Lorimer & Kramer 2005). Minimum companion masses were calculated assuming a 1.4 $M_\odot$ pulsar. The DM-derived distances were calculated using the NE2001 model of Galactic free electron density, and have typical errors of ∼20% (Cordes & Lazio 2002).
[a] These quantities are limits based on our error for $\dot{P}_{int}$ after correcting for the Shklovskii effect. See Section 5.2 for further details.
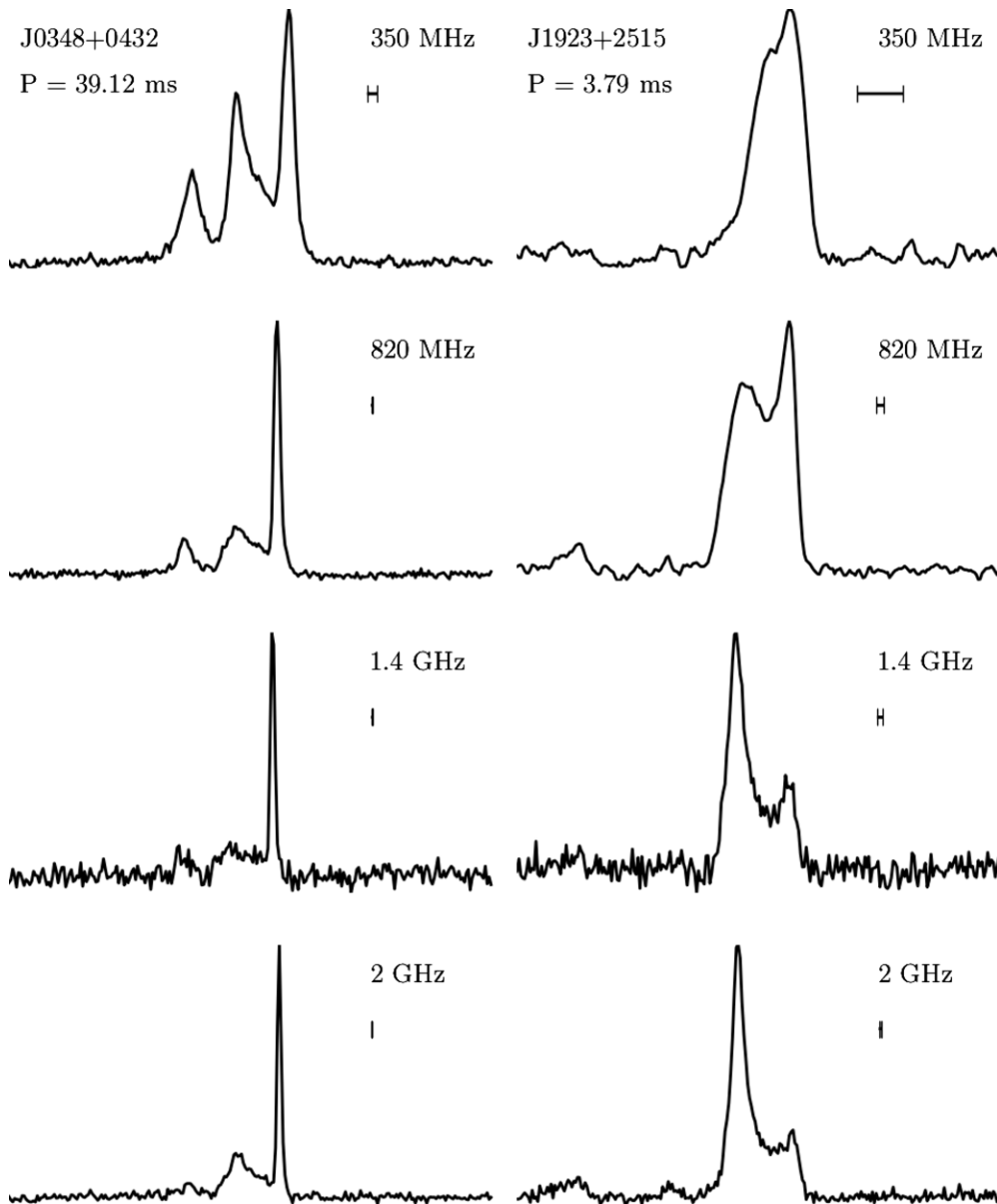
Figure 3. Integrated pulse profiles at four observing frequencies for the newly discovered recycled pulsars presented here. All profiles show one full rotation of the pulsar (i.e., from phase 0–1) with 256 phase bins. The summed profiles were made by aligning each folded profile using the TEMPO ephemeris and then adding all the RFI-free observations at the specified frequencies. The profile evolution in both pulsars is clear. The bars show the relative timescale for dispersive smearing at each frequency (see Equation (3)).

relativity and other theories of gravity. Specifically, theories that invoke a scalar gravitational field predict that J0348 will be a strong emitter of dipolar gravitational radiation because the very different binding energies of the neutron star and white dwarf will lead them to couple differently to the scalar field (e.g., Stairs 2003). Similar tests have been done with PSR J1141−6545 (Bhat et al. 2008), J1012+5307 (Lazaridis et al. 2009), and J1738+0333 (Freire et al. 2012), but J0348 is in a tighter, more relativistic orbit and likely has a less massive companion, so it will be a stronger probe of these effects. A full analysis of the spectroscopic observations of J0348 and their implications for alternative theories of gravity will be presented in Antoniadis et al. (2012).

J0348 shows significant profile evolution as a function of frequency (see Figure 3); at frequencies above 1.4 GHz, the main profile component becomes extremely narrow, with a duty cycle of ~1%. This has allowed us to obtain very precise pulse

arrival times—our rms timing residuals are 9.3 μs but at high frequencies individual TOA uncertainties can be $\lesssim$3 μs. We are continuing long-term timing of this pulsar using the Arecibo Observatory.

5.2. PSR J1923+2515

PSR J1923+2515 (hereafter J1923) is an isolated MSP with a 3.8 ms spin period. Figure 3 shows the integrated pulse profile of J1923 at several different frequencies and the evolution in the profile shape is clear. We see evidence for a weak interpulse in our summed 820 MHz and 2 GHz data. The timing of J1923 improved significantly at higher frequencies, where we were able to obtain TOAs with uncertainties $\lesssim$1 μs. J1923 is being regularly observed at Arecibo as part of the NANOGrav timing array for gravitational wave detection (Demorest et al. 2012). It will also be suitable for the European Pulsar Timing Array (van Haasteren et al. 2011).
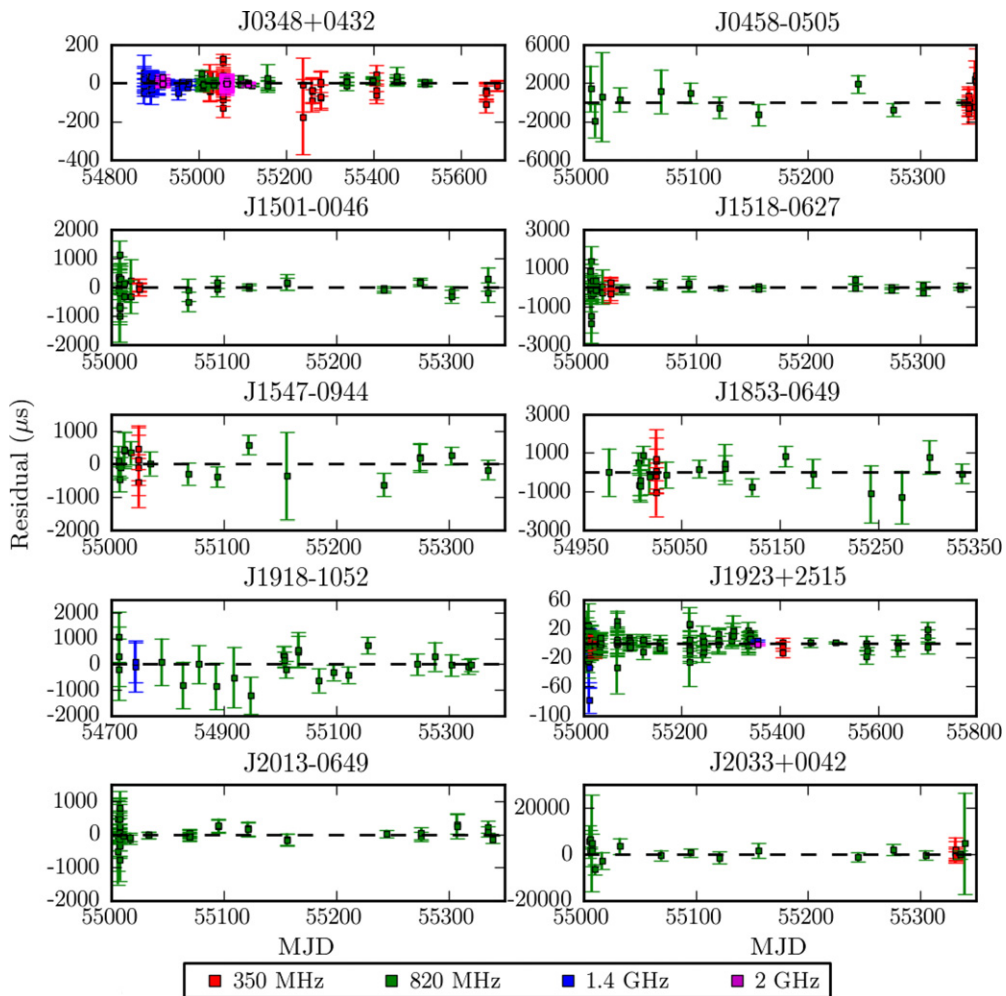
Figure 4. Post-fit timing residuals for each of the newly discovered pulsars. Only phase connected TOAs are shown. Nominal TOA errors have been multiplied by a constant error factor so that the reduced $\chi^2 = 1$. Note that the axes have different scales in most plots.

J1923 is the only pulsar presented here for which we were able to measure a significant proper motion. We find $\mu_\alpha = -6.2(1.2)$ mas yr^{-1} and $\mu_\delta = -23.6(3.5)$ mas yr^{-1}. We performed an F-test to determine if the addition of proper motion is in fact required by the data. The full χ^2 of our timing model excluding proper motion is 339.63, with 147 degrees of freedom. When proper motion is included in the fit, $\chi^2 = 146.02$ with 145 degrees of freedom. The probability that this improvement is due to chance is 1×10^{-16}. Thus, the improvement in our timing solution when proper motion is included is extremely significant. We used the DM and the NE2001 model of Galactic free electron density to estimate the distance to J1923, $D = 1.6(3)$ kpc, where the number in parentheses represents a 20% fractional error, which is typical for these estimates (Cordes & Lazio 2002). At this distance, the observed proper motion corresponds to a transverse velocity $v_\perp = 188(46)$ km s^{-1}, which is within the observed range of other MSPs, though higher than average (Gothoskar & Gupta 2000; Bogdanov et al. 2002; Gonzalez et al. 2011).

Using this $v_\perp$ we can calculate the magnitude of the Shklovskii effect (Shklovskii 1970):

$$\frac{\dot{P}_\mu}{P} = \frac{v_\perp^2}{c\,D}. \qquad (8)$$

We find $\dot{P}_\mu = 8.9(4.7) \times 10^{-21}$ s s^{-1}. Acceleration within the Galactic potential will also cause a bias in the observed

$\dot{P}$. We estimate this contribution following Nice & Taylor (1995), but find that biases due to acceleration perpendicular and parallel to the Galactic plane are only -3.3×10^{-22} s s^{-1} and -3.4×10^{-22} s s^{-1}, respectively. These are an order of magnitude smaller than $\dot{P}_\mu$. The bias due to the Shklovskii effect is 94% of the observed $\dot{P}$ and would imply that the intrinsic spin-down of the pulsar is $\dot{P}_{\rm int} = 0.6(4.7) \times 10^{-21}$ s s^{-1}, so we can only place an upper limit on $\dot{P}_{\rm int}$ at this time. A more precise measurement of proper motion or a better distance estimate will be needed to constrain the magnitude of the Shklovskii effect and to obtain a better measurement of $\dot{P}_{\rm int}$. In the meantime, the derived quantities listed in Table 3 are upper limits based upon our measurement uncertainties for $\dot{P}_{\rm int}$.

5.3. PSR J0458−0505

PSR J0458−0505 (hereafter J0458) is a nulling pulsar with a 1.9 s spin period. It was detected in both the Fourier domain and single-pulse searches. The profile is slightly asymmetric (see Figure 2), with a small trailing component. The reduced χ^2 obtained from our timing solution after fitting for position, P, $\dot{P}$, and DM was substantially higher than unity. As we see no systematic trends in our timing residuals, we assume that the number of pulses per individual observation was too small, due to a combination of a long period, limited integration time and a very large nulling fraction (NF, see below). The pulse profile thus probably did not stabilize within these TOA integrations. To
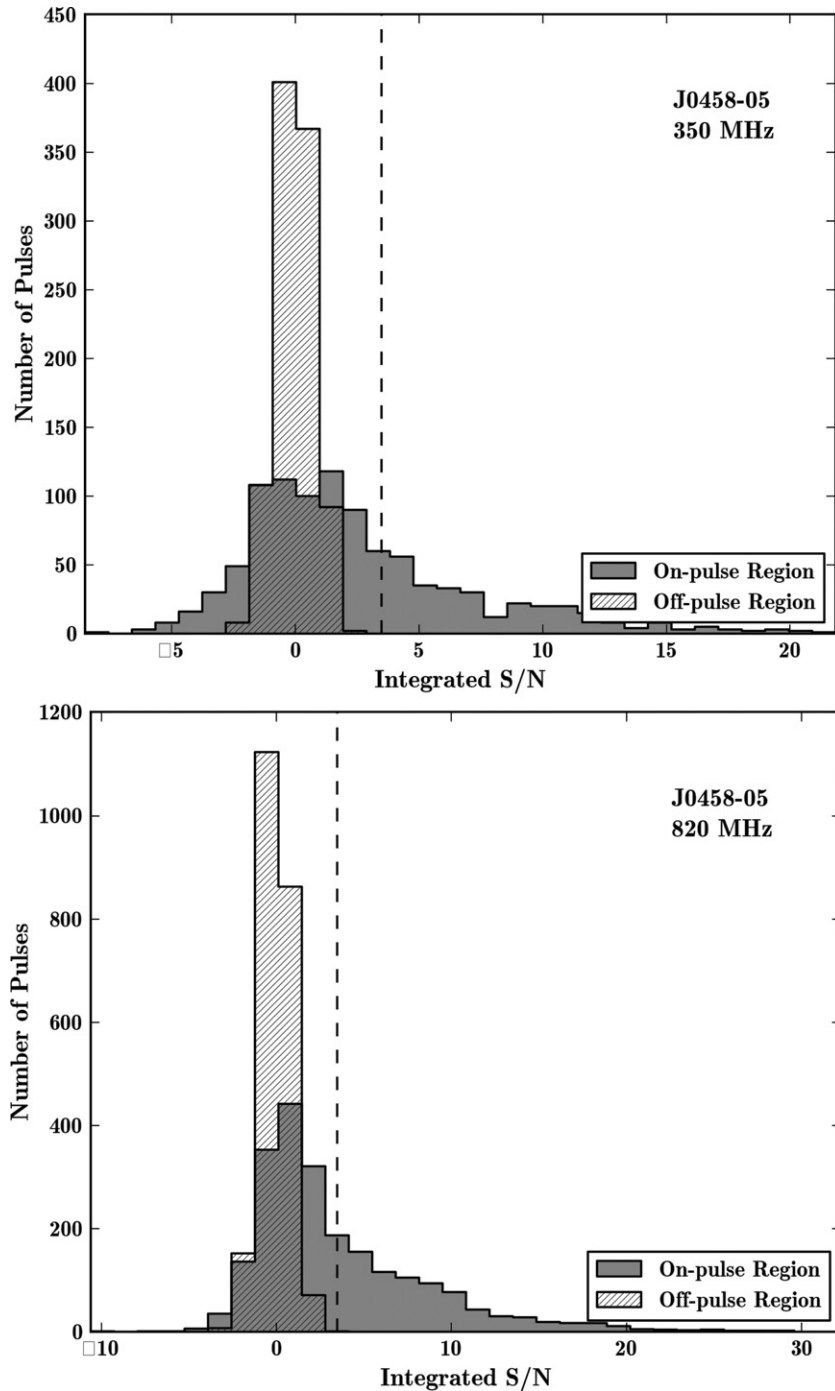
Figure 5. Histograms of integrated S/N for single pulses of J0458. The top panel is for data taken at 350 MHz, while the bottom panel is for data taken at 820 MHz. The on-pulse region is shown in gray and the off-pulse region as hatched. The dashed line shows the $S/N_{thresh} = 3.5$, above which we counted the pulsar as being in an "on" state.

make the reduced χ^2 equal to one, we multiplied our individual TOA errors by a constant factor of 2.97. Although we were still able to derive an accurate timing solution for J0458, the fractional errors in the timing parameters are larger than for most of the other pulsars presented here, especially for declination and $\dot{P}$.

5.3.1. Estimate of the Nulling Fraction

We estimate the NF of J0458 in the following way. We first removed strong sources of RFI from each observation. We then folded each data set using sub-integrations that were a single-

pulse period in duration using the `psrfits_singlepulse` command from `psrfits_utils`.[27] In some sub-integrations, systematic trends due to lower levels of RFI were still visible. To remove these, we used a least-squares minimization technique to fit up to a maximum of four independent sinusoids to the off-pulse region of each sub-integration and then subtracted them from the data, creating a flat off-pulse baseline. Each sub-integration was then normalized to have an off-pulse median and rms noise level of zero and one, respectively.

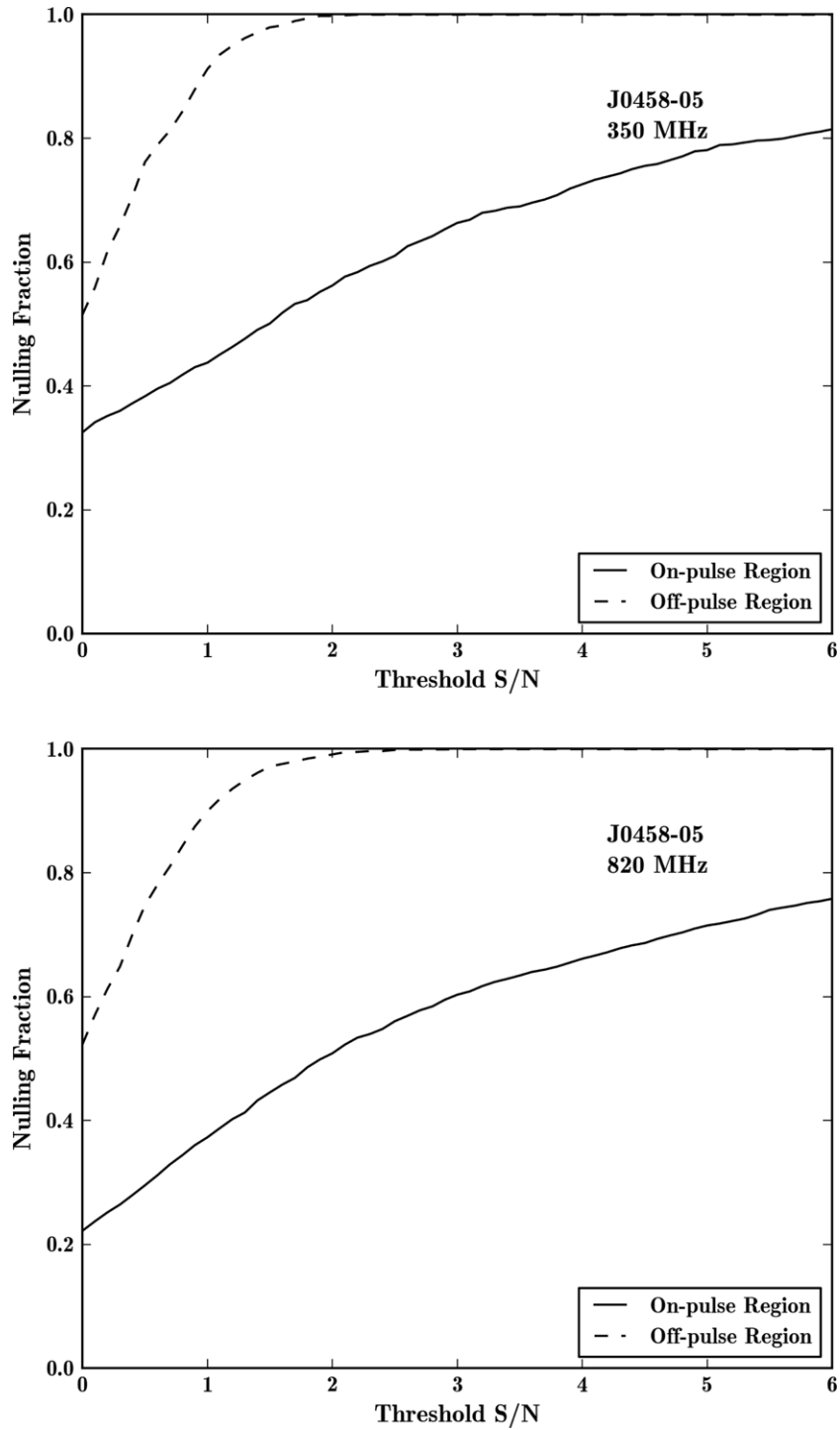[27] https://github.com/demorest/psrfits_utils

Figure 6. Nulling fraction of J0458 as a function of S/N_{thresh}. The top panel is for data taken at 350 MHz, while the bottom panel is for data taken at 820 MHz.

To determine if the pulsar was in an "on" state, we calculated the integrated S/N in the on-pulse region, which was determined by inspection of the integrated pulse profile. We also calculated the integrated S/N in an off-pulse region with the same number of bins as the on-pulse region. We counted a pulse as being in the "on" state if it had an integrated S/N above some threshold, S/N_{thresh}. We chose S/N_{thresh} based on the statistics of the off-pulse region. Histograms of the on-pulse and off-pulse S/Ns can be found in Figure 5, and in Figure 6 we show NF as a function of threshold S/N. Our calculations show that the off-pulse region rarely exceeded $S/N = 3.0$, as expected for Gaussian distributed

noise. To be conservative, we set $S/N_{thresh} = 3.5$, though we also report NF for $S/N_{thresh} = 3.0$ and 4.0 for comparison.

After removing RFI, J0458 was observed for a total of 2218 full rotations at 820 MHz and we find NF = [0.60, 0.63, 0.66] for $S/N_{thresh} = [3.0, 3.5, 4.0]$, respectively. J0458 was observed for a total of 978 rotations at 350 MHz with NF = [0.66, 0.69, 0.73] for $S/N_{thresh} = [3.0, 3.5, 4.0]$, respectively. These NFs are fairly high compared to other pulsars, but are not unprecedented—PSRs B1112+50 and B1944+17 have comparable NF (Ritchings 1976). The NF of J0458 seems to be similar at both 350 MHz and 820 MHz. This behavior is consistent
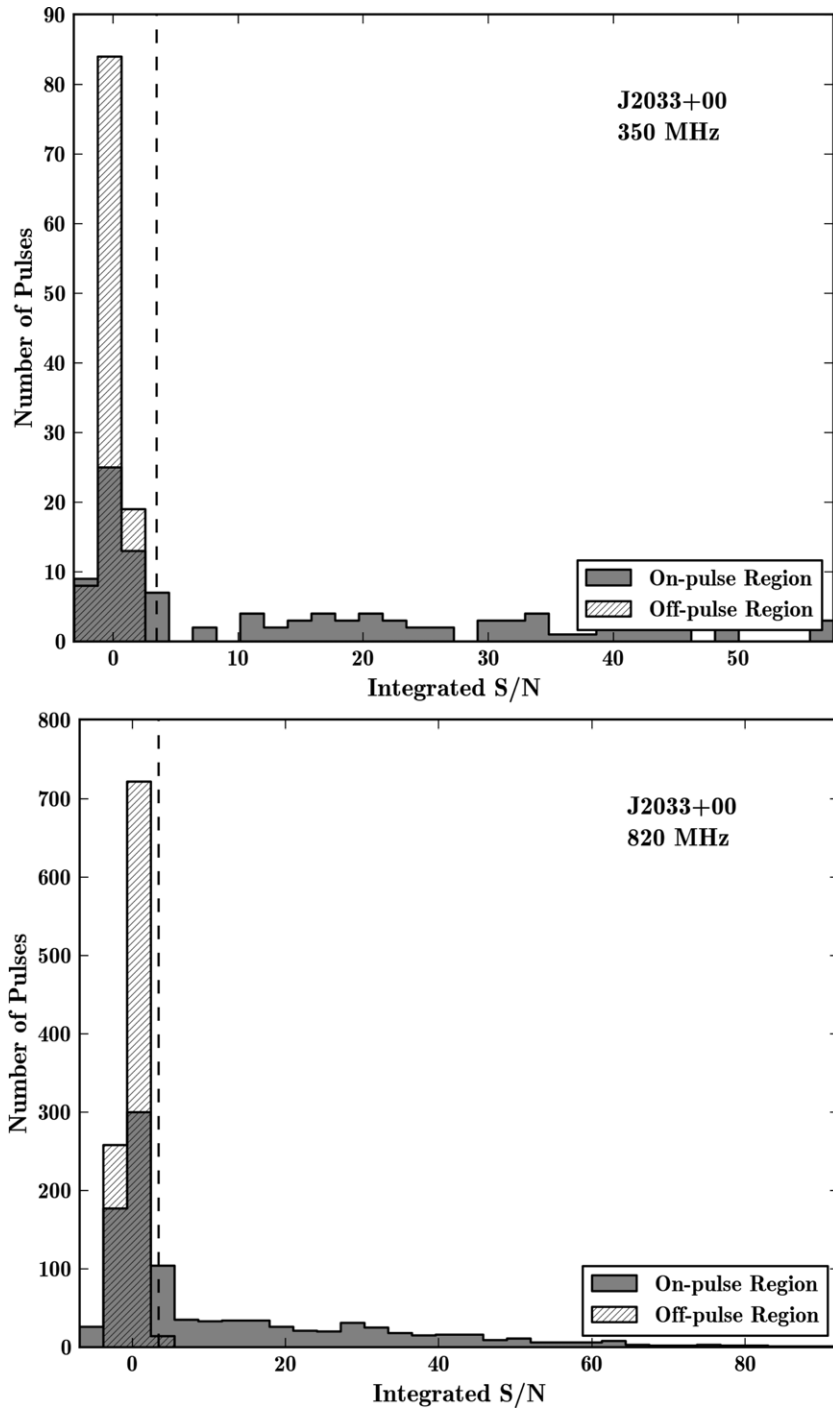
Figure 7. Histograms of S/N for single pulses of J2033. The data labels are the same as in Figure 5.

with previous studies that suggest nulling is a broadband phenomenon at low frequencies (see Biggs 1992 and references therein).

5.4. PSR J2033 + 0042

PSR J2033 + 0042 (hereafter J2033) is a 5.0 s pulsar that, like J0458, nulls significantly. It was reported by Burke-Spolaor & Bailes (2010) as an RRAT that sometimes was detected in Fourier searches. Burke-Spolaor & Bailes (2010) report on the position, period, and DM of J2033 and note its high NF and the presence of drifting sub-pulses. Here, we present a full timing solution and quantitative measurement of the NF. We

detected J2033 in both single-pulse and Fourier searches. Only 9 radio pulsars and 12 RRATs in the ATNF catalog have a longer period than J2033. Like J0458, the fractional errors in our timing parameters were relatively large, probably because our integration times were shorter than the pulse stabilization time. J2033 has a longer period than J0458 and also nulls significantly.

We used the same procedure as outlined in Section 5.3.1 to estimate the NF in J2033. We observed the pulsar for 994 rotations at 820 MHz and we find a NF = [0.53, 0.56, 0.58] for S/N_{thresh} = [3.0, 3.5, 4.0], respectively. J2033 was observed for 111 rotations at 350 MHz and we find NF = [0.44, 0.48, 0.49] for S/N_{thresh} = [3.0, 3.5, 4.0], respectively. Histograms of S/N can be found in Figure 7 and NF as a function of S/N_{thresh} is
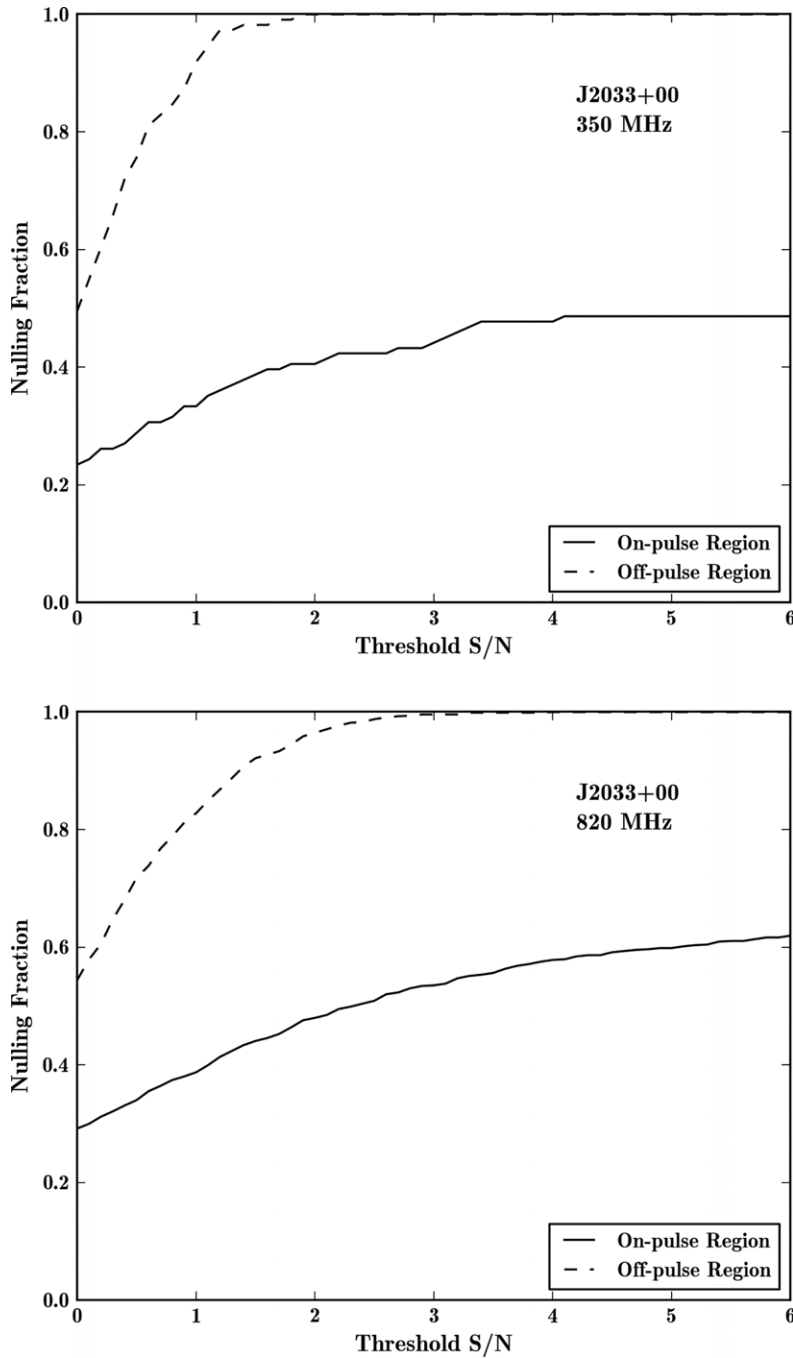
Figure 8. Nulling fraction of J2033 as a function of S/N_{thresh}. The data labels are the same as in Figure 6.

plotted in Figure 8. The NF of J2033 is somewhat higher at 820 MHz than at 350 MHz, but we only observed J2033 at 350 MHz on one occasion, so a more detailed study of the nulling characteristics of this pulsar should be conducted before drawing firm conclusions about the frequency dependence of NF. Overall, pulsars J0458 and J2033 are on less than half of the time, adding to a growing sub-population of pulsars that are mostly off (Keane et al. 2011).

6. CONCLUSION

The Drift-scan Survey has discovered 31 pulsars, 10 of which are presented here. The majority are isolated long-period pulsars. J0348 is a mildly recycled binary pulsar that has a low-mass white dwarf companion in a relativistic orbit. It is a unique and powerful system for testing gravitational theories and hence we are continuing to time it long term. A more detailed study of J0348 will be presented in Antoniadis et al. (2012). J1923 is an isolated MSP. We have a significant measurement of the pulsar's proper motion, but the implied magnitude of the Shklovskii effect is nearly equal to the observed spin-down, so we are only able to set limits on the rotational characteristics of J1923. Long-term monitoring should help to better constrain the proper motion and intrinsic spin-down. J0458 and J2033 are both nulling pulsars with NFs $\gtrsim$50%.

REFERENCES

Antoniadis, J., Freire, P. C. C., Wex, N., et al. 2012, Sci, submitted
Archibald, A. M., Kaspi, V. M., Bogdanov, S., et al. 2010, ApJ, 722, 88
Archibald, A. M., Stairs, I. H., Ransom, S. M., et al. 2009, Sci, 324, 1411
Bhat, N. D. R., Bailes, M., & Verbiest, J. P. W. 2008, PhRvD, 77, 124017
Biggs, J. D. 1992, ApJ, 394, 574
Bogdanov, S., Pruszyńska, M., Lewandowski, W., & Wolszczan, A. 2002, ApJ, 581, 495
Boyles, J., Lynch, R. S., Lorimer, D. R., et al. 2013, ApJ, 763, 80
Burke-Spolaor, S., & Bailes, M. 2010, MNRAS, 402, 855
Cordes, J. M., & Lazio, T. J. W. 2002, arXiv:astro-ph/0207156
Demorest, P. B., Ferdman, R. D., Gonzalez, M. E., et al. 2012, ApJ, in press (arXiv:1201.6641)
Dewey, R. J., Taylor, J. H., Weisberg, J. M., & Stokes, G. H. 1985, ApJL, 294, 25
DuPlain, R., Ransom, S., Demorest, P., et al. 2008, Proc. SPIE, 7019, 70191D
Freire, P. C. C., Wex, N., Esposito-Farèse, G., et al. 2012, MNRAS, 423, 3328
Gonzalez, M. E., Stairs, I. H., Ferdman, R. D., et al. 2011, ApJ, 743, 102
Gothoskar, P., & Gupta, Y. 2000, ApJ, 531, 345
Haslam, C. G. T., Salter, C. J., Stoffel, H., & Wilson, W. E. 1982, A&AS, 47, 1
Hessels, J. W. T., Ransom, S. M., Kaspi, V. M., et al. 2008, in AIP Conf. Proc. 983, 40 Years of Pulsars: Millisecond Pulsars, Magnetars and More, ed. C. Bassa, Z. Wang, A. Cumming, & V. M. Kaspi (Melville, NY: AIP), 613
Hotan, A. W., van Straten, W., & Manchester, R. N. 2004, PASA, 21, 302
Jenet, F., Finn, L. S., Lazio, J., et al. 2009, arXiv:0909.1058
Kaplan, D. L., Escoffier, R. P., Lacasse, R. J., et al. 2005, PASP, 117, 643
Keane, E. F., Kramer, M., Lyne, A. G., Stappers, B. W., & McLaughlin, M. A. 2011, MNRAS, 415, 3065
Lazaridis, K., Wex, N., Jessner, A., et al. 2009, MNRAS, 400, 805
Lorimer, D. R., & Kramer, M. 2005, Handbook of Pulsar Astronomy (Cambridge: Cambridge Univ. Press)
Lorimer, D. R., Yates, J. A., Lyne, A. G., & Gould, D. M. 1995, MNRAS, 273, 411
Morris, D. J., Hobbs, G., Lyne, A. G., et al. 2002, MNRAS, 335, 275
Nice, D. J., & Taylor, J. H. 1995, ApJ, 441, 429
Ransom, S. M. 2001, PhD thesis, Harvard Univ.
Ransom, S. M., Eikenberry, S. S., & Middleditch, J. 2002, AJ, 124, 1788
Ritchings, R. T. 1976, MNRAS, 176, 249
Rosen, R., Heatherly, S., McLaughlin, M. A., et al. 2010, AEdRv, 9, 010106
Shklovskii, I. S. 1970, SvA, 13, 562
Stairs, I. H. 2003, LRR, 6, 5
van Haasteren, R., Levin, Y., Janssen, G. H., et al. 2011, MNRAS, 414, 3117